DOI: 10.1002/ejic.200900046

Redox Modification of EMACs Through the Tuning of Ligands: Heptametal(II) Complexes of Pyrazine-Modulated Oligo-α-pyridylamido Ligands

Rayyat Huseyn Ismayilov,[a,b] Wen-Zhen Wang,[a,b] Gene-Hsiang Lee,[a] Chih-Hsien Chien,[a] Chien-Hong Jiang,[a] Chien-Lan Chiu,[c] Chen-Yu Yeh,[c] and Shie-Ming Peng*[a,b]

Keywords: Metal–metal interactions / Nickel / Chromium / Magnetic properties

Using pyrazine-modulated oligo-α-pyridylamido ligands N^2-(pyrazin-2-yl)-N^6-[6-(pyrazin-2-ylamino)pyridin-2-yl]pyridine-2,6-diamine (H_3pzpz) and N^2-(pyrazin-2-yl)-N^6-[6-(pyridin-2-ylamino)pyridin-2-yl]pyridine-2,6-diamine (H_3tpz), linear heptametal(II) extended metal atom chains (EMACs) $[M_7(\mu_7\text{-}L)_4X_2]$ [L = $pzpz^{3-}$, M = Ni^{II}, X = Cl^- (**1**), NCS^- (**2**); M = Cr^{II}, X = Cl^- (**3**), NCS^- (**4**); L = tpz^{3-}, M = Cr^{II}, X = Cl^- (**5**), NCS^- (**6**)] were synthesized and structurally characterized. Electrochemical studies showed that heptanickel(II) complexes can undergo one reversible oxidation at +0.46 V for **1** and +0.52 V for **2**. Chromium(II) species **3** exhibited two reversible, one-electron oxidation peaks at +0.61 and +0.88 V, and **5** exhibited three reversible, one-electron oxidation peaks at +0.40, +0.68 and +1.07 V. The redox peaks shifted positively when axial ligands changed from chloride to thiocyanate anions, at +0.67 and +0.92 V for **4** and +0.44, +0.73 and +1.11 V for **6**. The introduction of electron-withdrawing pyrazine rings to the spacer ligand retarded oxidation of the heptametal EMACs and stabilized the complexes. In nickel(II) species **1** and **2**, both terminal nickel atoms exist in spin state $S = 1$ whereas all the inner nickel atoms exist in spin state $S = 0$. Temperature-dependent magnetic research revealed an antiferromagnetic interaction between the two terminal atoms through a superexchange pathway along metal cores with a parameter of about $-4\ cm^{-1}$. Chromium(II) species **3**–**6** showed a localized structure consisting of three quadruple Cr–Cr bonds and a single terminal Cr^{II} atom. Magnetic study revealed a quintet ground state resulting from the isolated, high-spin Cr^{II} atom.

Introduction

Since the 1990s extended metal atom chain (EMAC) complexes have attracted much attention from inorganic chemists. The study of the metal–metal interactions in EMACs is invaluable for acquiring a fundamental understanding of metal–metal bonds. Some EMAC complexes show delocalized electronic structure and have potential applications such as molecular electronic devices.[1] A series of tri-,[2] tetra-,[3] penta-,[4] hexa-,[5] hepta-[6] and nonanuclear[7] EMAC complexes using oligo-α-pyridylamido ligands (Scheme 1) have been synthesized and studied. The typical structure of this family includes a linear metal chain, which is helically wrapped by four deprotonated oligo-α-pyridylamido ligands; all the pyridine nitrogen and amido nitrogen atoms are coordinated to the metal in a *syn* form. Most work in this area has been carried out by us and Cotton's group. Our current research in this field is heading in three directions: (1) Expanding the variety of metals. EMACs of Cu,[2f] Ni,[7a] Co,[2a,2c,6c] Cr,[2d,7b] Ru[2b,2g] and Rh[2b,2g] have been synthesized and structurally characterized. EMACs of other metals, for instance, first-row transition metals iron and manganese, rare-earth metals and so forth, have yet to be successfully synthesized. (2) Extending the length of molecules. Research in this area is strongly stimulated by the potential application of EMACs as molecular wires. Theoretically, when an EMAC contains enough metal atoms, the twisted, wrapping ligand will fulfil a single term around the metal array line and it is possible to extend the system to an infinite one-dimensional molecule. Work in this area is hindered by two factors: synthetic difficulty increases and yield decreases with an increase in the number of metal atoms and length of the molecules; the longer the EMAC is, the more easily it decomposes by oxidation.[8] The longest structurally characterized EMAC molecules obtained so far contain nine metal atoms for chromium and nickel[7] and seven metal atoms for cobalt.[6c] (3) Modulating the electronic structures and properties. Redox properties are especially interesting when EMACs function as molecular devices. Electron delocalization in the

[a] Department of Chemistry, National Taiwan University, Taipei, Taiwan, Republic of China
E-mail: smpeng@ntu.edu.tw
[b] Institute of Chemistry, Academia Sinica, Taipei, Taiwan, Republic of China
[c] Department of Chemistry, National Chung Hsing University, Taichung, Taiwan, Republic of China

metal chain through metal–metal bonds is crucial for electron conductivity, and the loss and gain of electrons provide bistable states, which are the basis for molecular switches. The electronic structure of EMACs depends on both the metal and ligands. Previous research on EMACs of oligo-α-pyridylamido ligands has revealed that nickel EMAC complexes are interpreted as localized molecules: both terminal nickel atoms exist in spin state $S = 1$ whereas all the inner nickel atoms exhibit spin state $S = 0$.[4d,4f] Cobalt and chromium EMACs showed significant metal–metal interaction and higher electron conductivity than those of nickel complexes.[1b,6c] On the other hand, modification of spacer ligands gives rise to a subtle change of molecular energy levels and consequently changes the redox properties of EMACs. We have designed a series of tuning oligo-α-pyridylamido ligands modified with pyrazine,[2e,6c,7b] naphthyridine[5] and toluenesulfonyl[9] and so forth instead of a pyridine ring. By using the tuning ligands, we have succeeded in not only synthesizing the longest EMACs so far obtained, such as nonachromium and heptacobalt EMACs, but also synthesizing many new EMACs with properties different from those of the oligo-α-pyridylamido ligand EMACs.

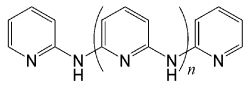

oligo-α-pyridylamido ligands

($n = 0$, Hdpa; $n = 1$, H_2tpda;

$n = 2$, H_3teptra)

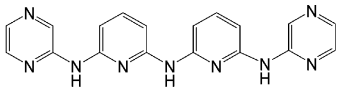

H_3pzpz

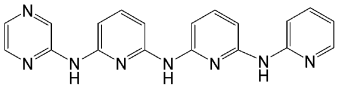

H_3tpz

Scheme 1.

Here we report heptanickel EMACs $[Ni_7(\mu_7\text{-pzpz})_4Cl_2]$ (**1**), $[Ni_7(\mu_7\text{-pzpz})_4(NCS)_2]$ (**2**) and heptachromium EMACs $[Cr_7(\mu_7\text{-pzpz})_4Cl_2]$ (**3**), $[Cr_7(\mu_7\text{-pzpz})_4(NCS)_2]$ (**4**), $[Cr_7(\mu_7\text{-tpz})_4Cl_2]$ (**5**) and $[Cr_7(\mu_7\text{-tpz})_4(NCS)_2]$ (**6**) of pyrazine-modulated tetrapyridyltriamine (H_3teptra) ligands N^2-(pyrazin-2-yl)-N^6-(6-(pyrazin-2-ylamino)pyridin-2-yl)pyridine-2,6-diamine (H_3pzpz) and N^2-(pyrazin-2-yl)-N^6-[6-(pyridin-2-ylamino)pyridin-2-yl]pyridine-2,6-diamine (H_3tpz).

Results and Discussion

Syntheses and Structures

The ligands H_3pzpz and H_3tpz were synthesized by palladium-catalyzed cross-coupling of aromatic amine and halide, and characterized by IR, ^{1}H NMR and MS(FAB).[6c]

The chloride EMACs **1**, **3** and **5** were synthesized when anhydrous MCl_2 reacted with corresponding ligands in argon using naphthalene as solvent and *t*BuOK as base to deprotonate the amine group. Our thiocyanate species **2**, **4** and **6** were obtained through the substitution of axial ligands from **1**, **3** and **5**. All the heptametal complexes **1**–**6** showed considerable solubility in common organic solvents, including both polar and nonpolar solvents. Selected bond lengths and angles are listed in Table 1. The crystal structures of **1**–**3**, **5** and **6** are shown in Figures 1, 2, 3, 4 and 5, respectively. Similar to complexes of oligo-α-pyridylamido ligands, molecules of all complexes showed EMAC structures: seven metal atoms were linear with M–M–M bond angles close to 180°; four all-deprotonated ligands, $pzpz^{3-}$ or tpz^{3-}, were wrapped around the metal string in *syn*-*syn* form as a heptadentate trianion helix. The lengths of the whole M_7 score in complexes **1**–**3**, **5** and **6** are 13–14 Å.

Molecules of **1** and **2** reside on a crystallographic site of twofold symmetry that is perpendicular to the nickel chain and goes through the central nickel atoms. The molecular structure of **1** is disordered because it is racemic and contains both *R* and *S* configurations of supporting ligands $pzpz^{3-}$, and each configuration exists at 50% probability. In complex **2**, there are two independent molecules; the structure of supporting ligands $pzpz^{3-}$ is not disordered but a sulfur atom in each axial ligand NCS^- is disordered on two equally occupied positions. The linearity of molecules **1** and **2** is excellent, with an average Ni–Ni–Ni bond angle of 179.6°. The N–Ni–Ni–N torsion angles for adjacent Ni^{II} are in the range 16–24°, and the average value of total torsion angles for one ligand [N–M(1)–M(7)–N] are 123° and 128° for **1** and **2**. The Ni–Ni distances in **1** and **2** lie in the range 2.2401–2.3839 Å, consistent with the values of nickel(II) EMACs of oligo-α-pyridylamido ligand.[6b,7a] An increase in Ni–Ni distances has been observed, from the central nickel atom to terminal nickel atoms, as occurred in other EMACs. The terminal nickel atoms are in five-coordinated pyramidal geometry with Ni–N_{av} distances of typical high-spin state of 2.089(18) and 2.095(6) Å for **1** and **2**, respectively. The inner nickel atoms are in four-coordinate square-planar conformation with Ni–N_{av} distances in the range 1.892(8)–1.917(5) Å, and consistent with low-spin Ni^{II}. A comparison of Ni–Ni distances among $[Ni_7(\mu_7\text{-pzpz})_4X_2]$ and $[Ni_7(\mu_7\text{-teptra})_4X_2]$ (X = Cl^-, NCS^-) complexes is shown in Scheme 2. It is noticeable that the innermost Ni–Ni bond [Ni(3)–Ni(4)] distances in EMACs $[Ni_7(\mu_7\text{-pzpz})_4X_2]$, which are 2.2516(7) and 2.2401(8) Å for **1** and **2**, respectively, are much longer than those of $[Ni_7(\mu_7\text{-teptra})_4X_2]$ [2.206(2)–2.225(2) Å].[6b] The distances between terminal nickel atoms and axial ligands [Ni–Cl 2.320(2) Å for **1** and Ni–N_{NCS} 2.036(6) Å for **2**] are shorter than those in $[Ni_7(\mu_7\text{-teptra})_4X_2]$ [Ni–Cl 2.364(3) Å and Ni–N_{NCS} 2.06(2) Å, respectively], maybe because of the two-pyrazine-containing ligand H_3pzpz providing a stronger ligand field than the unmodulated oligo-α-pyridylamido ligand H_3teptra.[6b,6c] This phenomenon was also observed in trinickel EMACs.[2e]

Heptachromium EMACs **3**–**6** are unstable in solution. Thiocyanate species **4** decomposed so quickly during X-ray analysis that we failed to collect enough diffraction data for high-quality structure resolution even though the data

Table 1. Selected bond lengths [Å] and angles [°] for **1**–**3**, **5** and **6**..[a]

1			
Ni(1)–Ni(2)	2.3839(12)	Ni(2)–Ni(3)	2.2870(11)
Ni(3)–Ni(4)	2.2516(7)	Ni(1)–N_{av}	2.089(18)
Ni(2)–N_{av}	1.897(14)	Ni(3)–N_{av}	1.911(6)
Ni(4)–N_{av}	1.896(15)	Ni(1)–Cl(1)	2.320(2)
Ni(1)–Ni(2)–Ni(3)	179.42(6)	Ni(2)–Ni(3)–Ni(4)	179.84(7)
Ni(3)–Ni(4)–Ni(3A)[b]	179.73(8)	Cl(1)–Ni(1)–Ni(2)	179.69(10)
2			
Ni(1)–Ni(2)	2.3674(11)	Ni(2)–Ni(3)	2.2906(10)
Ni(3)–Ni(4)	2.2483(7)	Ni(5)–Ni(6)	2.3694(11)
Ni(6)–Ni(7)	2.2748(11)	Ni(7)–Ni(8)	2.2319(8)
Ni(1)–N_{av}	2.098(6)	Ni(2)–N_{av}	1.897(5)
Ni(3)–N_{av}	1.917(5)	Ni(4)–N_{av}	1.908(5)
Ni(5)–N_{av}	2.092(6)	Ni(6)–N_{av}	1.899(5)
Ni(7)–N_{av}	1.914(5)	Ni(8)–N_{av}	1.892(8)
Ni(1)–N(19)	2.028(6)	Ni(5)–N(39)	2.044(6)
Ni(1)–Ni(2)–Ni(3)	179.14(5)	Ni(2)–Ni(3)–Ni(4)	179.98(6)
Ni(3)–Ni(4)–Ni(3A)[c]	179.45(7)	Ni(5)–Ni(6)–Ni(7)	179.19(5)
Ni(6)–Ni(7)–Ni(8)	179.88(6)	Ni(7)–Ni(8)–Ni(7A)[c]	179.96(7)
N(19)–Ni(1)–Ni(2)	179.9(2)	Ni(6)–Ni(5)–N(39)	178.42(18)
3			
Cr(1)–Cr(2)	2.072(2)	Cr(2)–Cr(3)	2.639(3)
Cr(3)–Cr(4)	1.832(6)	Cr(4)–Cr(3B)	2.593(6)
Cr(3B)–Cr(2B)	1.854(3)	Cr(2B)–Cr(1A)[d]	2.501(2)
Cr(1)–$N_{av.}$	2.104(4)	Cr(2)–$N_{av.}$	2.029(4)
Cr(3)–$N_{av.}$	2.060(4)	Cr(4)–$N_{av.}$	2.033(10)
Cr(1)–Cl(1)	2.4907(16)		
Cr(1)–Cr(2)–Cr(3)	177.49(10)	Cr(2)–Cr(3)–Cr(4)	178.2(4)
Cr(3)–Cr(4)–Cr(3B)	178.1(5)	Cr(4)–Cr(3B)–Cr(2B)	178.8(4)
Cr(3B)–Cr(2B)–Cr(1A)[d]	177.93(11)	Cl(1)–Cr(1)–Cr(2)	179.14(7)
Cr(2B)–Cr(1A)–Cl(1A)[d]	178.74(6)		
5			
Cr(1)–Cr(2)	2.160(7)	Cr(2)–Cr(3)	2.521(7)
Cr(3)–Cr(4)	2.087(6)	Cr(4)–Cr(3B)	2.328(5)
Cr(3B)–Cr(2B)	1.944(7)	Cr(2B)–Cr(1B)	2.415(7)
Cr(1)–$N_{av.}$	2.091(11)	Cr(2)–$N_{av.}$	2.033(17)
Cr(3)–$N_{av.}$	2.048(10)	Cr(4)–$N_{av.}$	2.020(15)
Cr(1)–Cl(1)	2.462(6)	Cr(1B)–Cl(1)	2.545(5)
Cr(1)–Cr(2)–Cr(3)	179.7(3)	Cr(2)–Cr(3)–Cr(4)	176.3(3)
Cr(3)–Cr(4)–Cr(3B)	177.3(3)	Cr(4)–Cr(3B)–Cr(2B)	175.5(3)
Cr(3B)–Cr(2B)–Cr(1B)	179.3(4)	Cl(1)–Cr(1)–Cr(2)	173.5(3)
Cr(2B)–Cr(1B)–Cl(1)	173.1(3)		
6			
Cr(1)–Cr(2)	2.456(3)	Cr(2)–Cr(3)	1.909(5)
Cr(3)–Cr(4)	2.548(5)	Cr(4)–Cr(3B)	1.892(5)
Cr(3B)–Cr(2B)	2.557(5)	Cr(2B)–Cr(1)	2.100(4)
Cr(1)–$N_{av.}$	2.111(15)	Cr(2)–$N_{av.}$	2.029(12)
Cr(3)–$N_{av.}$	2.055(18)	Cr(4)–$N_{av.}$	2.028(14)
Cr(1)–N(19)	2.199(6)		
Cr(1)–Cr(2)–Cr(3)	179.4(2)	Cr(2)–Cr(3)–Cr(4)	179.5(2)
Cr(3)–Cr(4)–Cr(3B)	179.48(19)	Cr(4)–Cr(3B)–Cr(2B)	179.5(2)
Cr(3B)–Cr(2B)–Cr(1)	179.9(2)	Cr(2B)–Cr(1)–N(19)	179.5(2)
Cr(2)–Cr(1)–N(19)	179.47(19)		

[a] Bond lengths of M–N_{av} represent the average value of M–N from the four wrapping ligands and label B represents nonsymmetric related positions (disordered positions). [b] Symmetry operation for **1**: A = *–x* + 1, *–y*, *z*. [c] Symmetry operation for **2**: A = *–x* + 1, *–y* + 1, *z*. [d] Symmetry operation for **3**: A = *–x* + 1, *y*, *–z* + 1/2.

clearly showed seven chromium atoms in a chain. However, thiocyanate EMACs are very important for the measurement of electron conductivity. Therefore we synthesized heptachromium thiocyanate with one-pyrazine-modulated tetrapyridyltriamine (H_3teptra) ligand and successfully obtained its crystal structure. This is the first example of heptachromium thiocyanate EMAC structure.

Molecules **3**, **5** and **6** reside on a crystallographic site of twofold symmetry that is perpendicular to the metal chain and goes through the centre of the molecule. Cr(2), Cr(3)

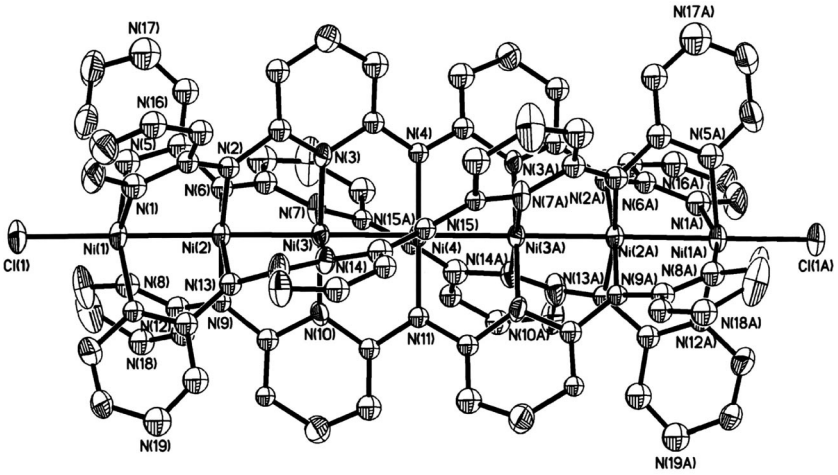

Figure 1. Crystal structure of $[Ni_7(\mu_7\text{-pzpz})_4Cl_2]$ (**1**). The hydrogen atoms have been omitted for clarity and thermal ellipsoids are at the 30% probability level. Symmetry operations A = $-x + 1, -y, z$.

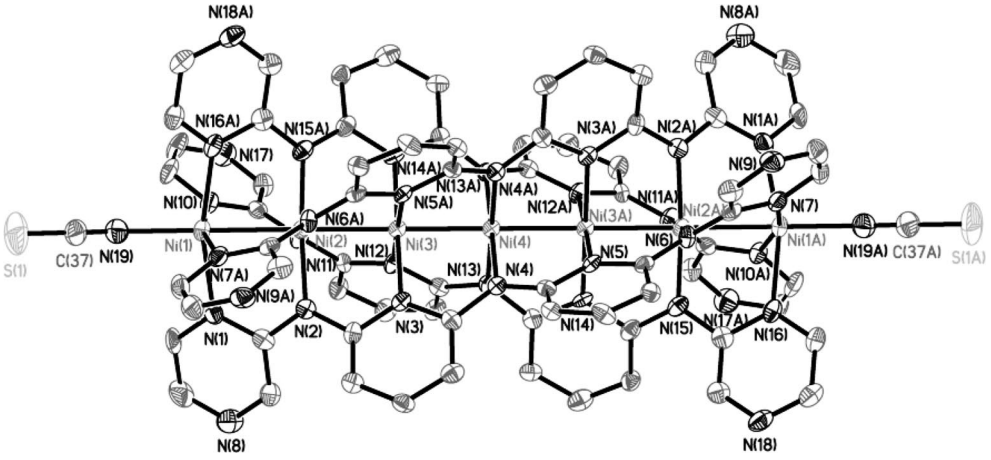

Figure 2. Crystal structure of one $[Ni_7(\mu_7\text{-pzpz})_4(NCS)_2]$ (**2**) molecule. The hydrogen atoms have been omitted for clarity and thermal ellipsoids are at the 50% probability level. Symmetry operations A = $-x + 1, -y + 1, z$.

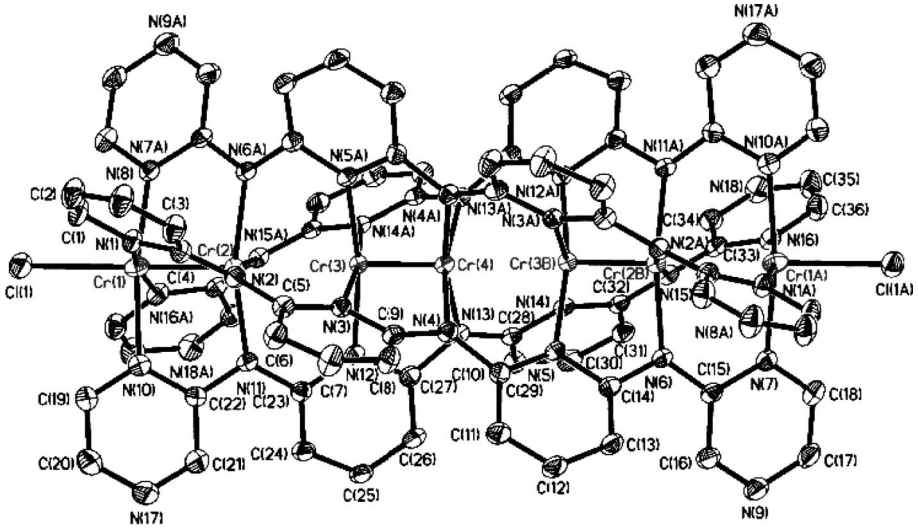

Figure 3. Crystal structure of $[Cr_7(\mu_7\text{-pzpz})_4Cl_2]$ (**3**). The hydrogen atoms have been omitted for clarity. Label A was generated through the symmetry operations A = $-x + 1, y, -z + 1/2$ and label B represents nonsymmetric related positions (disordered positions). The thermal ellipsoids are at the 30% probability level.

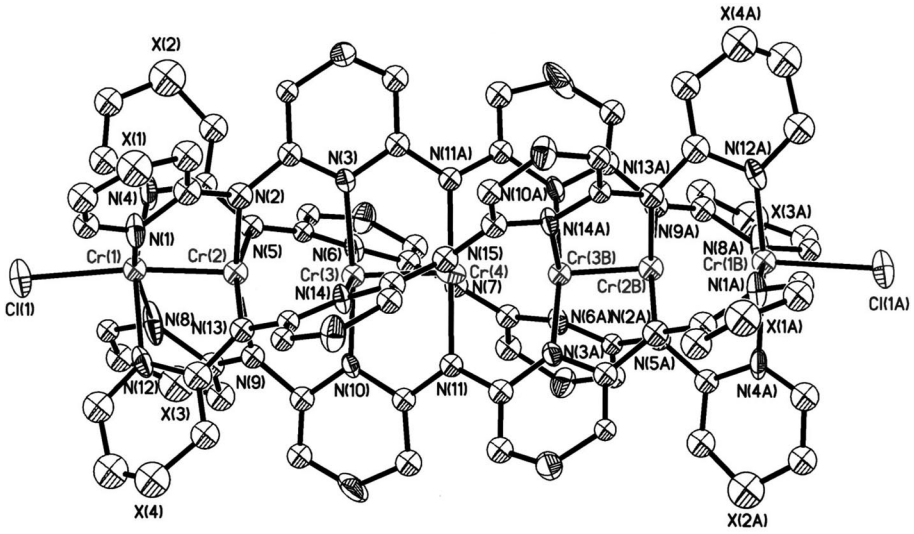

Figure 4. Crystal structure of $[Cr_7(\mu_7\text{-tpz})_4Cl_2]$ (**5**). Label A was generated through the symmetry operations A = $-x$, y, $-z + 1/2$ and label B represents nonsymmetric related positions (disordered positions). The hydrogen atoms have been omitted for clarity and thermal ellipsoids are at the 30% probability level.

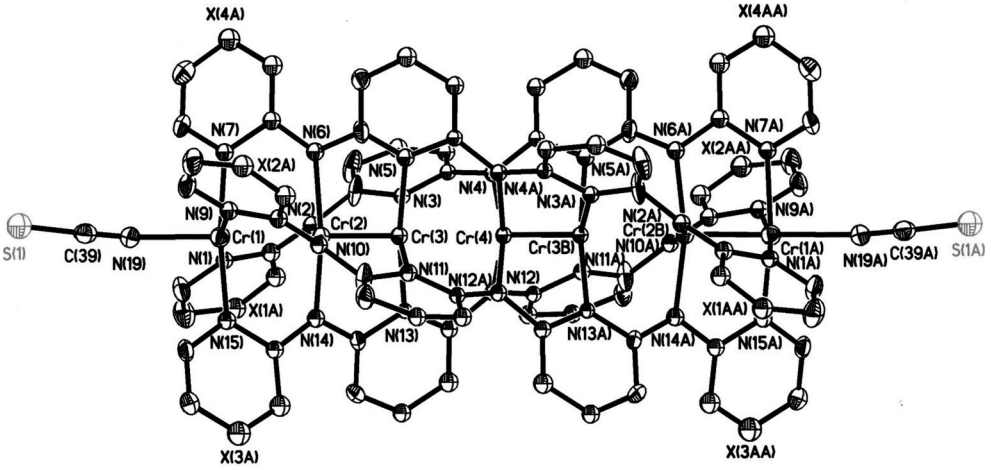

Figure 5. Crystal structure of $[Cr_7(\mu_7\text{-tpz})_4(NCS)_2]$ (**6**). The hydrogen atoms have been omitted for clarity. Label A was generated through the symmetry operations A = $-x$, y, $-z + 1/2$ and label B represents nonsymmetric related positions (disordered positions). The thermal ellipsoids are at the 30% probability level.

and Cr(4) atoms in **3** and **6** and Cr(1), Cr(2) and Cr(3) atoms in **5** are disordered on two positions and each position is half occupied. The supporting ligands in **5** and **6** are disordered in both *R* and *S* configurations and each configuration exists in equal probability. The probability of pyrazine or pyridine for each terminal aromatic ring is 50% because of the technical limit of discriminating between nitrogen and carbon atoms. The sulfur atom of axial ligand NCS^- in **6** is disordered on two equally occupied positions, as in **2**. The linearity of molecules **3**, **5** and **6** is excellent, with Cr–Cr–Cr bond angles in the range 175–180°; the average is 178.1, 177.6 and 179.6° for **3**, **5** and **6**, respectively. The average value of total torsion angles for one ligand [N–M(1)–M(7)–N] is about 118, 138 and 119° for **3**, **5** and **6**, respectively.

Two kinds of structures, with symmetrical and unsymmetrical configurations, have been found for trichromium EMAC, and transformation of the two types of structures was observed when EMACs underwent oxidation.[2d,2e,2h,4e] The symmetrical structures showed delocalized electronic structure and all Cr–Cr bonds exhibited equivalent or very close distances of $d_{Cr-Cr} > 2.3$ Å. The unsymmetrical structures showed localized electronic structure consisting of quadruple Cr–Cr bond(s) with $d_{Cr-Cr} < 2.3$ Å and a separated chromium atom. For EMACs with pyrazine-modulated oligo-α-pyridylamido ligands, the trichromium complex $[Cr_3(\mu_3\text{-dpza})_4Cl_2]$ [Hdpza = bis(2-pyrazyl)amine] showed symmetrical structure but nonachromium complexes $[Cr_9(\mu_9\text{-}N_9\text{-mpz})_4X_2]$ {H_4N_9-mpz = N^2,N^6-bis[6-(pyridin-2-ylamino)pyridin-2-yl]pyrazine-2,6-diamine, X = Cl^-, NCS^-} showed unsymmetrical structure.[2e,7b] In heptachromium EMACs **3**, **5** and **6**, Cr–Cr bond lengths fall into two categories. The shorter one is in the range 1.832(6)–2.160(7) Å, indicating clear quadruple Cr–Cr bonds. The

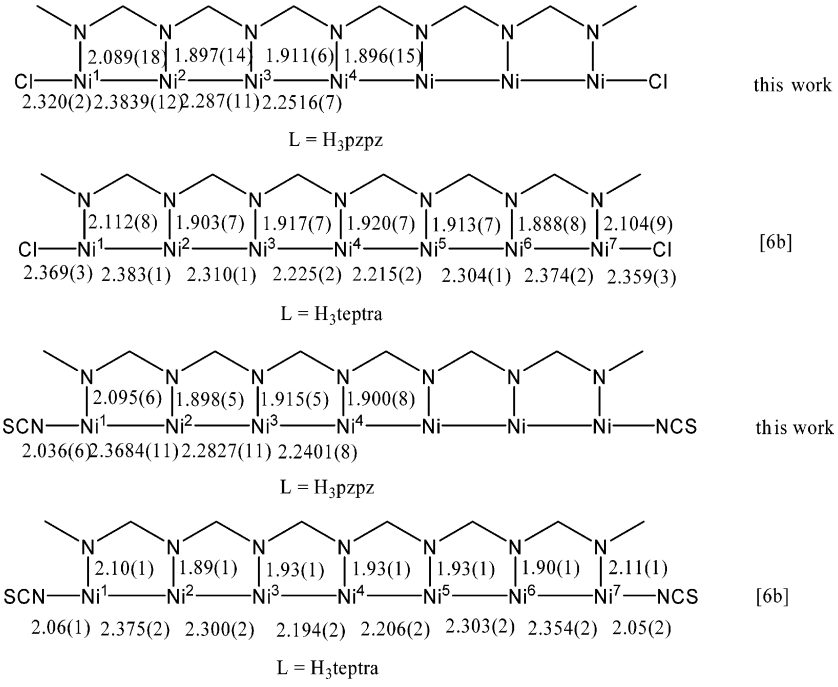

Scheme 2. Comparison of bond lengths in heptanickel(II) EMACs.

longer Cr–Cr distances range from 2.328(5) to 2.639(3) Å. Thus complexes **3**, **5** and **6** are composed of three quadruple Cr–Cr bonds and a single terminal Cr^{II} atom coordinated in a pyramidal X–Cr–N_4 unit (for **3** and **5**, X = Cl^-; for **6**, X = NCS^-), and the three quadruple Cr–Cr bonds and the single Cr^{II} are aligned in a straight chain. This is different from the complex of unsubstituted ligand [$Cr_7(\mu_7$-teptra)$_4$-Cl_2], in which Cr–Cr distances are close and the electrons are delocalized over the whole molecular chain.[6a] This may be because pyrazine-modulated ligands favour unsymmetrical structure. The Cr–Cl bond lengths [2.4907(16) Å for **3** and 2.504(6) Å for **5**] are shorter than that in [$Cr_7(\mu_7$-teptra)$_4$-Cl_2] [average 2.551(3) Å], as happened in the trichromium complex [$Cr_3(\mu_3$-dpza)$_4Cl_2$] and heptanickel complexes **1** and **2**.

The charge distributions and π bond orders of supporting ligand anions $pzpz^{3-}$ and tpz^{3-} were studied and calculated based on the resonance analysis (Scheme 3). Negative charges were restrained only on the coordinated nitrogen atoms to simplify the calculation. Bond lengths from X-ray crystallographic structure are in good agreement with the theoretical calculation. In all the EMACs the terminal nitrogen atom has the least negative density and terminal M–N bond lengths are the longest in all the M–N bonds of the molecules (M = Ni, Cr). The negative densities on amido nitrogen atoms [N(2) and N(4)] are higher than those on nitrogen atoms of aromatic rings [N(1) and N(3)] and consequently M–N_{amido} bonds [M(2)–N(2) and M(4)–N(4)] are significantly stronger and bond lengths shorter than those

Table 2. Comparison of C–C and C–N bond lengths.[a]

Complex	1	2	3
N(1)–C(1)	1.356(18)	1.348(9)	1.357(6)
N(1)–C(4)	1.359(19)	1.352(9)	1.353(6)
N(2)–C(4)	1.386(18)	1.368(9)	1.361(6)
N(2)–C(5)	1.393(15)	1.386(9)	1.388(6)
N(3)–C(5)	1.346(19)	1.370(9)	1.365(6)
N(3)–C(9)	1.402(17)	1.365(9)	1.370(6)
N(4)–C(9)	1.390(17)	1.383(9)	1.378(6)
X(1)–C(2)	1.348(3)	1.344(10)	1.339(8)
X(1)–C(3)	1.304(19)	1.313(9)	1.321(7)
C(1)–C(2)	1.337(19)	1.376(11)	1.361(8)
C(3)–C(4)	1.408(2)	1.414(10)	1.424(7)
C(5)–C(6)	1.357(3)	1.384(9)	1.388(7)
C(6)–C(7)	1.373(19)	1.385(10)	1.382(8)
C(7)–C(8)	1.418(18)	1.373(11)	1.375(7)
C(8)–C(9)	1.375(2)	1.395(9)	1.394(7)

[a] The labelling is according to Scheme 3. The bond lengths are average values from the four supporting ligands.

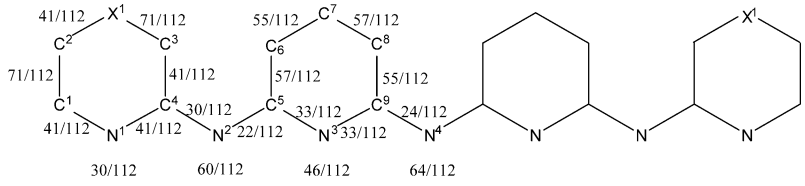

Scheme 3. Negative charge distribution and π bond orders of ligand anions, $pzpz^{3-}$ and tpz^{3-}. X(1) = N in **1**–**3**. For **5** and **6**, the occupancy of X(1) is 50% for nitrogen and 50% for carbon.

of M–$N_{aromatic}$ bonds [M(1)–N(1) and M(3)–N(3)] in all the EMACs. As seen in Scheme 3, among all C–N and C–C bonds, π bond orders on N(2)–C(5) and N(4)–C(9) are the lowest and the bond lengths are the longest in each molecule. The bonds with the highest π bond order are X(1)–C(3) and C(1)–C(2); both bonds have the strongest π bond character and their bond lengths are shortest (Table 2).

Electrochemistry

EMACs have exhibited very rich redox chemistry. Some of the multinuclear complexes showed more than two stable states, which provide the basis of their potential application as molecular wires and switches.[1b] Research on EMACs has revealed that their electrochemical properties depended on the type and numbers of metal ions, and that the introduction of electron-withdrawing or donor groups also gives rise to a change of redox properties. For EMACs of oligo-α-pyridylamido ligands with the same metal, we found that the longer the metal chain was, the lower the first oxidation potential was, and therefore the more easily it underwent oxidation.[8] EMACs of pyrazine-modulated ligands (H_3pzpz and H_3tpz) showed very different electrochemical properties from those of the oligo-α-pyridylamido ligand H_3teptra. The cyclic voltammograms of complexes **1**, **3** and **5** in solutions of CH_2Cl_2 are shown in Figure 6 and the electrochemical data are summarized in Table 3. Both of the heptanickel(II) complexes showed only one reversible, one-electron oxidation peak, at +0.46 and +0.52 V for **1** and **2**, respectively. The values are much higher than the first oxidation peaks for $[Ni_7(\mu_7\text{-teptra})_4X_2]$ (0.18 and 0.17 V for X = Cl^- and NCS^-, respectively), revealing that introduction of an electron-withdrawing group pyrazine to the supporting ligand retards oxidation of the metal chain, which is consistent with trinickel(II) complexes.[2e]

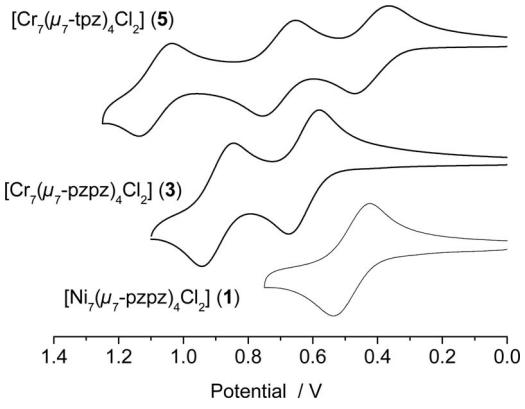

Figure 6. Cyclic voltammograms of **1**, **3** and **5** in CH_2Cl_2 containing 0.1 M TBAP.

The spectral changes for oxidation of **1** in CH_2Cl_2 containing 0.1 M TBAP were performed at various applied potentials from 0.42 to 0.60 V (Figure 7). Upon the increase of applied potentials, absorption bands at 245, 285, 554 and 629 nm decreased and those at 395 and 891 nm increased with isosbestic points at 235, 262, 277, 365, 410 and 658 nm. The clear isosbestic points indicated that no intermediates were produced during the oxidation process. An increase of absorption intensity of the near IR region was observed as a broad band centred at 1135 nm, which can be ascribed to the intervalence charge transfer of mixed-valence species Ni_7^{15+}. The oxidation of **2** in CH_2Cl_2 containing 0.1 M TBAP was also performed at various applied potentials from 0.43 to 0.63 V (Figure 7). The absorption bands at 245, 285, 545 and 627 nm decreased, and those at 400, 849 nm and near IR increased with isosbestic points at 260, 365, 411 and 660 nm as the applied potentials increased from 0.43 to 0.63 V. The near IR absorption centred at 1110 nm corresponded to the intervalence charge transfer of species Ni_7^{15+}.

Table 3. Redox potentials [V] for heptametal EMACs **1**–**6**.

Complexes	Oxidation				Reduction
	4th	3rd	2nd	1st	1st
1				+0.46	
2				+0.52	
3			+0.88	+0.61	
4			+0.92	+0.67	
5		+1.07	+0.68	+0.40	
6		+1.11	+0.73	+0.44	
$[Ni_7(\mu_7\text{-teptra})_4Cl_2]$[6b]			+0.73	+0.18	
$[Ni_7(\mu_7\text{-teptra})_4(NCS)_2]$[6b]		+1.02	+0.79	+0.17	–0.95
$[Cr_7(\mu_7\text{-teptra})_4Cl_2]$[8]	+1.30	+0.94	+0.48	+0.27	

Heptachromium complex **3** exhibited two reversible, one-electron oxidation peaks at +0.61 and +0.88 V, and **5** exhibited three reversible, one-electron oxidation peaks at +0.40, +0.68 and +1.07 V. The redox peaks shifted positively when axial ligands changed from chloride to thiocyanate anions, at +0.67 and +0.92 V for **4** and +0.44, +0.73 and +1.11 V for **6**, which is consistent with that of heptanickel(II) complexes **1** and **2** and with the previous results.[2e,7b,8] According to the research on $[Cr_3(\mu_3\text{-dpa})_4Cl_2]$ [Hdpa = bis(2-pyridyl)amine] and $[Cr_5(\mu_5\text{-tpda})_4Cl_2]$ [H_2tpda = *N*,*N*′-bis(2-pyridyl)-2,6-diaminopyradine], the first oxidation corresponded to the loss of one electron from isolated Cr^{II} and the resulting species was Cr_7^{15+} with the backbone shown below.[2h,4e,10]

In the cyclic voltammograms, $[Ni_7(\mu_7\text{-teptra})_4Cl_2]$ showed two oxidation peaks, and $[Ni_7(\mu_7\text{-teptra})_4(NCS)_2]$ showed three oxidation peaks and one reduction peak.[8] Compared with the heptametal EMACs of oligo-α-pyridylamido ligand H_3teptra, the first oxidation potential of **1**–**3** in the cyclic voltammogram increased more than 0.3 V. Thus the introduction of two electron-withdrawing pyrazine rings to the spacer ligand H_3teptra retarded oxidation of the heptametal EMACs and stabilized the complexes, which is consistent with our previous research and may be attributed to the fact that the pyrazine ring is more electronega-

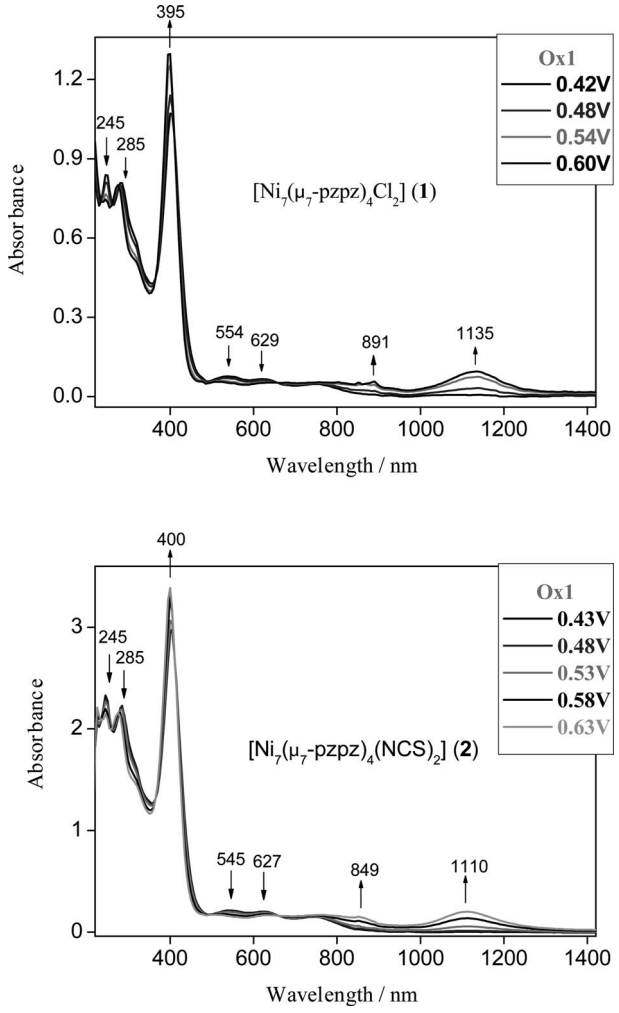

Figure 7. Spectral changes for oxidation of **1** (top) and **2** (bottom) in CH_2Cl_2 with 0.1 M TBAP at various applied potentials.

tive than the pyridine ring.[2e] It is noticeable that one-pyrazine-modulated species **5** exhibited three reversible oxidation peaks, and its first oxidation (+0.400 V) is lower than the two-pyrazine-modulated species **3** (+0.608 V) but higher than the unmodulated complex $[Cr_7(\mu_7\text{-teptra})_4Cl_2]$ (+0.27 V). This corresponds to the two forms of molecules, that is, an isolated terminal chromium atom may coordinate with pyridyl or pyrazyl ring, and one-pyrazine-modulated ligand H_3tpz has lower electron-withdrawing ability than two-pyrazine-modulated one H_3pzpz.

The spectral changes for oxidation of **4** in CH_2Cl_2 containing 0.1 M TBAP were performed at various applied potentials from 0.41 to 0.80 V (Figure 8). Upon the increase of applied potentials, absorption bands at 277, 343, 422 and 712 nm decreased and those at 385 and 587 nm increased. The clear isosbestic points at 361, 409, 476, 682 and 735 nm indicated that no intermediates were produced during the oxidation process. An increase of absorption intensity of the near IR region was observed as a broad band centred at 1223 nm, which can be ascribed to the intervalence charge transfer of mixed-valence species Cr_7^{15+}.

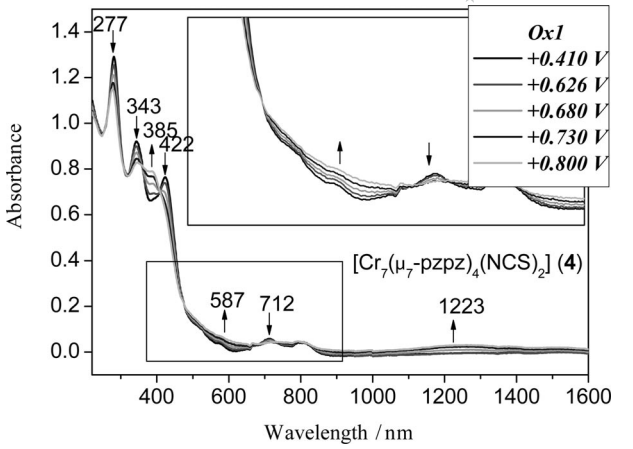

Figure 8. Spectral changes for oxidation of **4** in CH_2Cl_2 with 0.1 M TBAP at various applied potentials.

Magnetic Properties

The magnetic susceptibility of complexes **1** and **2** was measured over a temperature range of 2–300 K. The magnetic behaviour of heptanickel EMACs is similar and showed maximum magnetic susceptibilities of both compounds at 5 K for **1** and 6 K for **2** (Figure 9). The μ_{eff} values of **1** and **2** at room temperature (300 K) were 4.49 and 4.29 μ_B, respectively, corresponding to high-spin dinuclear nickel(II) complexes (uncoupled spin-only value of μ_{eff} is 4.00 μ_B). Therefore the magnetic results were consistent with the structural conclusion that both the terminal nickel(II) atoms are in spin state $S = 1$ and the five inner nickel(II) atoms are in spin state $S = 0$. As the temperature was lowered, the μ_{eff} values decreased, typical of antiferromagnetic behaviour. The temperature dependence of the magnetic susceptibility of **1** and **2** was fitted with a theoretical expression (1) for a dinuclear system deduced from the spin Hamiltonian equation $\boldsymbol{H} = -J\mathbf{S}_1\mathbf{S}_2$ ($S_1 = S_2 = 1$) and modified to include a number of uncoupled species, ρ. Molecular field correction was applied to take into account the MFA (mean-field approximation) as zj' for the interpret-

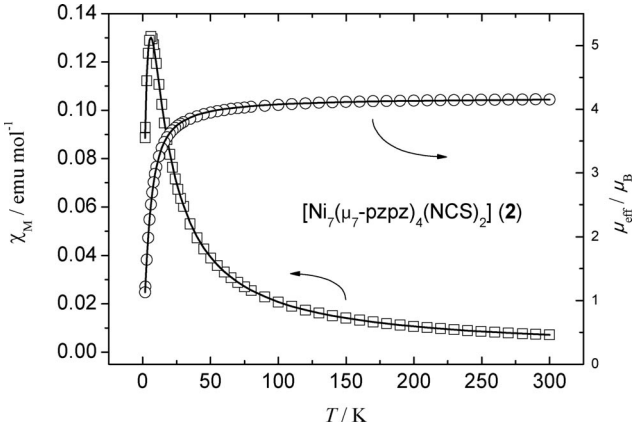

Figure 9. Plots of molar magnetic susceptibility χ_M (□, left) and μ_{eff} (○, right) vs. T for compound **2**. Solid lines result from least-squares fits using Equations (1) and (2).

ation of the magnetic interaction between metal string molecules [Equations (1) and (2)]. In both cases TIP corrections were included.

$$\chi = \frac{2Ng^2\beta^2(e^{J/kT}+5e^{3J/kT})}{kT(1+3e^{J/kT}+5e^{3J/kT})} \quad (1)$$

$$\chi_\rho = \chi(1-\rho)+\frac{2Ng^2\beta^2\rho}{3kT}S(S+1)+TIP \quad (2)$$

Least-squares fitting of the experimental data was in excellent agreement with the theoretical analyses and led to g = 2.16, J = –4.24, ρ = 0.076, zj' = –0.28 cm^{-1} and F = 1.05×10^{-5} for **1**, and g = 2.09, J = –4.69, ρ = 0.044, zj' = –0.22 cm^{-1} and F = 4.05×10^{-6} for **2** [F was defined as $\Sigma(\chi_{i(exp)})^{-1}(\chi_{i(exp)} - \chi_{i(theo)})^2$]. The resultant J values were consistent with the theoretical analyses of maximum magnetic susceptibilities according to $kT_{max}/|J|$ = 0.976 for the S = 1 system. In spite of the existence of two pyrazine rings and thus the different electron density in the bridging ligands, the magnetic coupling parameters were comparable with the reference's value for $[Ni_7(\mu_7\text{-teptra})_4Cl_2]$ (J = –3.8 cm^{-1}),[6b] which suggests that the magnetic interaction occurred through the aligned nickel atoms through a superexchange mechanism.

The magnetic behaviour of the heptachromium(II) EMACs **3**–**6** was similar (Table 4). The magnetic moments and susceptibilities of **4** are depicted as a function of temperature in Figure 10. The magnetic moments of complexes **3**–**6** at room temperature (300 K) were 4.97–5.10 μ_B, respectively, which corresponded to a quintet ground state. As all the quadruple-bonded Cr^{II} atoms are diamagnetic, the magnetic contribution of heptachromium EMACs **3**–**6** is due to the isolated terminal high-spin Cr^{II}. From 15 K to 300 K, μ_{eff} was almost constant. A fit of $1/\chi_M$ versus T with Curie–Weiss equation for S = 2 gave g = 2.03–2.09 and θ = –3.9 to –6.9 K. An obvious decrease of μ_{eff} was observed below 15 K because of zero-field splitting and intermolecular interactions. The θ values indicated both large magnitude of intermolecular interaction and zero-field splitting resulting from a strong interaction of electrons with delocalized molecular orbitals.

Table 4. Magnetic results for heptachromium complexes **3**–**6**.

Complexes	**3**	**4**	**5**	**6**
g	2.09	2.03	2.06	2.08
θ [K]	–5.5	–3.9	–6.9	–4.5
μ_{eff} at 300 K [μ_B]	5.06	4.97	5.07	5.10

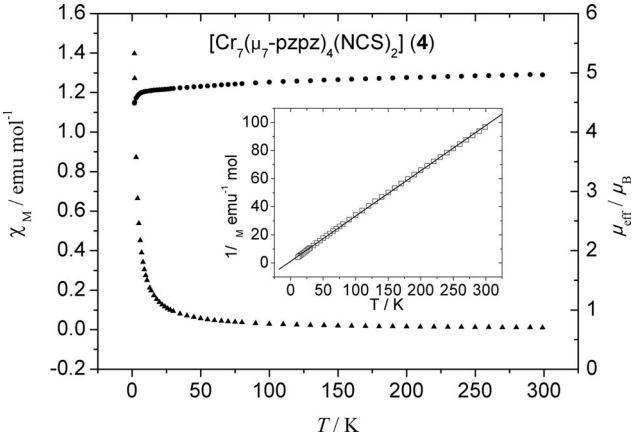

Figure 10. Plots of molar magnetic susceptibility χ_M (▲, left) and magnetic moment μ_{eff} (●, right) vs. T for compound **4**. Inset: Reciprocal dependence of the magnetic susceptibility on temperature. The solid lines result from least-square fits of the Curie–Weiss law.

Conclusions

In summary, we obtained single crystals of heptanickel(II) and heptachromium(II) EMAC complexes with pyrazine-modulated tetrapyridyltriamine ligands. The structural research showed that all the complexes were composed of seven metal atoms in line wrapped by four all-deprotonated ligands. In heptanickel(II) complexes **1** and **2** both terminal nickel atoms exist in spin state S = 1 whereas all the inner nickel atoms exhibit spin state S = 0. Magnetic study revealed that the magnetic interaction parameters between the terminal nickel atoms in **1** and **2** were about –4 cm^{-1}, and that supported a superexchange pathway through metal scores. Heptachromium(II) EMAC complexes showed localized structure consisting of three quadruple Cr–Cr bonds and a single terminal Cr^{II} atom. Magnetic studies revealed a quintet ground state resulting from the isolated, high-spin Cr^{II} atom. Electrochemical studies on **1** and **2** showed both heptanickel(II) complexes exhibited only one reversible, one-electron oxidation peak at +0.46 V for **1** and +0.52 V for **2**. Two-pyrazine-modulated heptachromium(II) complexes **3** and **4** exhibited two reversible, one-electron oxidation peaks, whereas one-pyrazine-modulated heptachromium(II) complexes **5** and **6** exhibited three reversible, one-electron oxidation peaks. No reduction was observed for heptanickel(II) and heptachromium(II) EMACs **1**–**6**. The introduction of electron-withdrawing pyrazine rings to the spacer ligands retarded oxidation of the heptanickel(II) and heptachromium(II) EMACs and stabilized the complexes.

Experimental Section

Materials: All reagents and solvents were obtained from commercial sources and were used without further purification unless otherwise noted. The CH_2Cl_2 used for electrochemistry was freshly distilled prior to use. Tetra-*n*-butylammonium perchlorate (TBAP) was recrystallized twice from ethyl acetate and dried under vacuum.

Physical Measurements: Absorption spectra were recorded with a Hewlett–Packard 8453 spectrophotometer. IR spectra were performed with a Perkin–Elmer FTIR Spectrometer PARAGON 1000 in the range 400–4000 cm^{-1}. FAB-MS mass spectra were obtained with a JEOL JMS-700 HF double focusing spectrometer operating in the positive-ion detection mode. Molar magnetic susceptibility was recorded with a SQUID system with 2000 Gauss external magnetic field. Electrochemistry was performed with a three-electrode potentiostat (CH Instruments, Model 750A) in CH_2Cl_2 deoxygenated by purging with prepurified nitrogen gas. Cyclic voltamme-

try was conducted with the use of a home-made three-electrode cell equipped with a BAS glassy carbon (0.07 cm^2) or platinum (0.02 cm^2) disk as the working electrode, a platinum wire as the auxiliary electrode and a home-made Ag/AgCl (saturated) reference electrode. The reference electrode was separated from the bulk solution by a double junction filled with electrolyte solution. Potentials were reported versus Ag/AgCl (saturated) and referenced to the ferrocene/ferrocenium (Fc/Fc^+) couple, which occurs at $E_{1/2}$ = +0.54 V versus Ag/AgCl (saturated). The working electrode was polished with 0.03 μm aluminium on Buehler felt pads and was put under ultrasonic radiation for 1 min prior to each experiment. The reproducibility of individual potential values was within ±5 mV. The spectroelectrochemical experiments were accomplished with the use of a 1-mm cuvette, a 100-mesh platinum gauze as working electrode, a platinum wire as the auxiliary electrode and a Ag/AgCl (saturated) reference electrode.

Preparation of Compounds

$[Ni_7(\mu_7\text{-pzpz})_4Cl_2]$ (1): Anhydrous $NiCl_2$ (635 mg, 4.90 mmol), H_3pzpz (500 mg, 1.40 mmol) and naphthalene (40 g) were placed in an Erlenmeyer flask. The mixture was heated (about 170–180 °C) overnight under argon. Then a solution of potassium *tert*-butoxide (565 mg, 5.0 mmol) in *n*-butyl alcohol (5 mL) was added dropwise. The mixture was refluxed until the remaining *n*-butanol evaporated completely. The product was transferred to hexane for washing out naphthalene after being cooled and then CH_2Cl_2 (100 mL) was used to extract the complex. A dark green complex was obtained after evaporation. The single crystals suitable for X-ray diffraction were obtained from slow evaporation of ether to a CH_2Cl_2 solution (226 mg, 34% yield). IR (KBr) $\tilde{\nu}$ = 3432 (m, br), 3070 (w), 2967 (w), 1586 (m), 1560 (m), 1443 (m), 1420 (m), 1396 (s), 1339 (s), 1326 (m), 1266 (w), 1230 (w), 1152 (s), 1053 (w), 1021 (m), 773 (w), 750 (w), 734 (w), 708 (w), 668 (w), 444 (w) cm^{-1}. UV/Vis (CH_2Cl_2) λ_{max} (ε, $dm^3\,mol^{-1}\,cm^{-1}$) = 249 (9.92×10^4), 284 (9.26×10^4), 319 (6.79×10^4), 404 (1.27×10^5), 539 (1.04×10^4), 624 (9.47×10^3), 749 (6.35×10^3) nm. MS (FAB): *m*/*z* (%) = 1898 (100) $[M]^+$. $C_{76}H_{58}Cl_2N_{36}Ni_7O$ [**1**·$C_2H_5OC_2H_5$] (1973.27): calcd. C 46.26, H 2.96, N 25.55; found C 45.92, H 2.75, N 25.26.

$[Ni_7(\mu_7\text{-pzpz})_4(NCS)_2]$ (2): $[Ni_7(\mu_7\text{-pzpz})_4Cl_2]$ (76 mg, 0.04 mmol) and NaNCS (16 mg, 0.20 mmol) were placed in an Erlenmeyer flask in CH_2Cl_2 (50 mL). The green solution was stirred for 2 d and filtered. Then water (20 mL) was added to dissolve the unreacted NaNCS. The solution was extracted with CH_2Cl_2 (3 × 60 mL). Na_2SO_4 was added to the organic layer to remove the water. The CH_2Cl_2 solution was evaporated to dryness and gave a dark green compound. The dark green single crystals suitable for X-ray diffraction were obtained from slow evaporation of ether to a chloroform solution after 2 weeks (56 mg, 73% yield). IR (KBr) $\tilde{\nu}$ = 3425 (m, br), 3070 (w), 2967 (w), 2068 (m), 1586 (m), 1553 (m), 1502 (m), 1442 (m), 1420 (s), 1396 (s), 1339 (s), 1326 (m), 1264 (w), 1229 (w), 1152 (s), 1021 (m), 773 (w), 750 (w), 734 (w), 708 (w), 668 (w), 445 (w) cm^{-1}. UV/Vis (CH_2Cl_2): λ_{max} (ε, $dm^3\,mol^{-1}\,cm^{-1}$) = 248 (1.14×10^5), 285 (1.07×10^5), 319 (7.74×10^4), 404 (1.45×10^5), 542 (1.15×10^4), 626 (1.09×10^4), 742 (7.98×10^3) nm. MS (FAB): *m*/*z* (%) = 1943 (20) $[M]^+$. $C_{75}H_{49}Cl_3N_{38}Ni_7S_2$ [**2**·$CHCl_3$] (2063.79): calcd. C 43.65, H 2.39, N 25.79; found: C 43.84, H 2.40, N 25.21.

$[Cr_7(\mu_7\text{-pzpz})_4Cl_2]$ (3): Anhydrous $CrCl_2$ (497 mg, 4.04 mmol), H_3pzpz (500 mg, 1.40 mmol) and naphthalene (45 g) were heated at about 170–180 °C under argon and then a solution of potassium *tert*-butoxide (565 mg, 5.0 mmol) in *n*-butyl alcohol (4 mL) was added dropwise. The reaction was continued for another 6 h. The product was transferred to hexane to wash out naphthalene after being cooled and then CH_2Cl_2 (200 mL) was used to extract the complex. A dark red-brown complex was obtained after evaporation. The product was recrystallized from a $CHCl_3$/diethyl ether solution (1:5). Deep red-brown crystals were obtained (266 mg, 43% yield). IR (KBr) $\tilde{\nu}$ = 3460 (m), br), 1586 (w), 1553 (m), 1522 (m), 1420 (s), 1396 (m), 1341 (m), 1262 (m), 1156 (m), 1026 (w), 781 (w), 445 (w) cm^{-1}. UV/Vis (CH_2Cl_2): λ_{max} (ε, $dm^3\,mol^{-1}\,cm^{-1}$) = 230 (6.19×10^4), 281 (7.97×10^4), 341 (5.71×10^4), 421 (5.01×10^4), 520 (7.95×10^3), 578 (3.25×10^3), 710 (5.16×10^3), 793 (3.56×10^3) nm. MS (FAB): *m*/*z* (%) = 1849 (100) $[M]^+$, 1813 (90) $[M - Cl]^+$. $C_{73}H_{52}Cl_2Cr_7N_{36}O$ [**3**·CH_3OH] (1884.31): calcd. C 46.53, H 2.78, N 26.76; found: C 46.87, H 2.58, N 26.73.

$[Cr_7(\mu_7\text{-pzpz})_4(NCS)_2]$ (4): $[Cr_7(\mu_7\text{-pzpz})_4Cl_2]$ (205 mg, 0.11 mmol) and NaNCS (72 mg, 0.89 mmol) in $CHCl_3$ (100 mL) were stirred for 2 d. The solvent was removed under reduced pressure. The remaining deep brown solid was extracted with CH_2Cl_2 (2 × 40 mL) and the solution was then layered with hexane. After 2 weeks deep red-brown crystals suitable for X-ray diffraction were obtained (128 mg, 61% yield). IR (KBr) $\tilde{\nu}$ = 3086 (m), 2849 (w), 2646 (w), 2044 (s), 1588 (s), 1554 (m), 1496 (m), 1472 (m), 1443 (s), 1418 (s), 1338 (s), 1260 (m), 1208 (w), 1155 (s), 1027 (m), 843 (w), 778 (m), 750 (w), 734 (w), 640 (w), 456 (w) cm^{-1}. UV/Vis (CH_2Cl_2): λ_{max} (ε, $dm^3\,mol^{-1}\,cm^{-1}$) = 248 (7.21×10^4), 280 (1.12×10^5), 346 (6.92×10^4), 423 (6.18×10^4), 523 (9.08×10^3), 585 (4.82×10^3), 714 (7.19×10^3), 794 (4.48×10^3) nm. MS (FAB): *m*/*z* (%) = 1896 (10) $[M]^+$, 1839 (20) $[M - NCS]^+$, 1326 (60) $[Cr_5(pzpz)_3]^+$. $C_{74}H_{48}Cr_7N_{38}S_2$ (1897.53): calcd. C 46.84, H 2.55, N 28.05; found C 46.57, H 2.72, N 28.08.

$[Cr_7(\mu_7\text{-tpz})_4Cl_2]$ (5): Compound **5** was synthesized using a procedure similar to that for **3** except that H_3tpz was used instead of H_3pzpz; yield 40%. IR (KBr) $\tilde{\nu}$ = 3447 (m), 1603 (m), 1582 (m), 1550 (m), 1472 (m), 1447 (m), 1410 (vs), 1353 (s), 1326 (m), 1197 (m), 1156 (s), 1118 (m), 1020 (m), 850 (w), 779 (m), 736 (m), 668 (m) cm^{-1}. UV/Vis (CH_2Cl_2): λ_{max} (ε, $dm^3\,mol^{-1}\,cm^{-1}$) = 233 (9.87×10^4), 283 (1.30×10^5), 341 (9.79×10^4), 408 (8.75×10^4), 724 (7.81×10^3) nm. MS (FAB): *m*/*z* (%) = 1850 (30) $[M]^+$, 1814 (100) $[M - Cl]^+$. $C_{76}H_{52}Cl_2Cr_7N_{32}$ (1848.32): calcd. C 49.39, H 2.84, N 24.25; found C 49.02, H 3.20, N 23.81.

$[Cr_7(\mu_7\text{-tpz})_4(NCS)_2]$ (6): Compound **6** was synthesized using a procedure similar to that for **4** except that **4** was used instead of **3**; yield 57%. IR (KBr): $\tilde{\nu}$ = 3086 (w), 3031 (w), 2837 (w), 2640 (w), 2036 (m), 1603 (m), 1586 (m), 1547 (m), 1494 (m), 1473 (m), 1446 (m), 1418 (s), 1400 (s), 1339 (s), 1305 (m), 1261 (m), 1237 (m), 1155 (s), 1023 (m), 1012 (m), 777 (m), 732 (m), 455 (m) cm^{-1}. UV/Vis (CH_2Cl_2): λ_{max} (ε, $dm^3\,mol^{-1}\,cm^{-1}$) = 229 (2.40×10^5), 283 (2.73×10^5), 343 (2.03×10^5), 405 (1.79×10^5), 719 (8.80×10^3) nm. $C_{80.5}H_{57}Cl_5Cr_7N_{34}S_2$ [**6**·$2.5CH_2Cl_2$] (2105.91): calcd. C 45.91, H 2.73, N 22.61; found: C 45.64, H 3.10, N 22.12.

Crystal Structure Determinations: The chosen crystals were mounted on a glass fibre. Data collection was carried out on a NONIUS Kappa CCD diffractometer at 150(1) K using Mo-K_α radiation (λ = 0.71073 Å) and a liquid-nitrogen low-temperature controller. Cell parameters were retrieved and refined using DENZO-SMN software on all reflections. Data reduction was performed on DENZO-SMN software. Semiempirical absorption was based on symmetry-equivalent reflections and absorption corrections were applied with the DENZO-SMN program. All the structures were solved using SHELXL-97 and refined with SHELXL-97 by full-matrix least-squares on F^2 values.[11,12] The crystal data for compounds **1**–**3**, **5** and **6** are listed in Table 5.

CCDC-706785 (for **1**), -706786 (for **2**), -706787 (for **3**), -706788 (for **5**) and -706789 (for **6**) contain the supplementary crystallographic data for this paper. These data can be obtained free of charge from

Table 5. Crystal data for **1**–**3**, **5** and **6**.

	1·2$C_2H_5OC_2H_5$·H_2O	**2**·1.5$C_2H_5OC_2H_5$·$CHCl_3$	**3**·3$C_2H_5OC_2H_5$	**5**·$C_2H_5OC_2H_5$	**6**·2$C_2H_5OC_2H_5$·3C_6H_6
Empirical formula	$C_{80}H_{70}Cl_2N_{36}Ni_7O_3$	$C_{81}H_{64}Cl_3N_{38}Ni_7O_{1.5}S_2$	$C_{84}H_{78}Cl_2Cr_7N_{36}O_3$	$C_{80}H_{62}Cl_2Cr_7N_{32}O$	$C_{104}H_{90}Cr_7N_{34}O_2S_2$
Formula mass	2065.59	2175.14	2074.72	1922.52	2276.22
Crystal system	orthorhombic	orthorhombic	orthorhombic	monoclinic	monoclinic
Space group	$P2_12_12$	$P2_12_12$	*Pbcn*	*P*2/*c*	*C*2/*c*
a [Å]	12.8370(4)	23.6382(3)	21.2470(4)	13.7594(4)	44.0057(9)
b [Å]	33.2169(6)	17.8446(2)	23.3850(4)	10.4976(4)	10.2244(2)
c [Å]	10.2744(14)	20.6812(2)	17.9490(4)	28.7980(9)	26.9041(5)
β [°]	90	90	90	93.2328(17)	125.3658(7)
V [Å^3]/*Z*	4381.1(6)/2	8723.63(17)/4	8918.2(3)/4	4153.0(2)/2	9871.3(3)/4
D_{calcd} [Mgm^{-3}]	1.566	1.656	1.545	1.537	1.532
Absorption coefficient [mm^{-1}]	1.603	1.690	0.952	1.013	0.855
Crystal size [mm]	0.40×0.40×0.20	0.25×0.20×0.20	0.40×0.10×0.02	0.20×0.12×0.02	0.30×0.15×0.08
θ range for data collection [°]	1.23–27.50	1.31–27.50	1.72–27.50	1.42–25.00	1.13–25.00
Reflections collected	25625	57224	54604	17859	27083
Independent reflections	9748 (R_{int} = 0.0532)	19846 (R_{int} = 0.0526)	10235 (R_{int} = 0.0668)	7329 (R_{int} = 0.0704)	8672 (R_{int} = 0.0723)
R_F, R_W (F^2) [$I>2\sigma(I)$]	0.0724, 0.2055	0.0575, 0.1660	0.0688, 0.1893	0.1001, 0.2805	0.0958, 0.2900
R_F, R_W (F^2) (all data)	0.1243, 0.2442	0.1109, 0.1945	0.1376, 0.2320	0.2203, 0.3466	0.1934, 0.3489
Gof	1.042	1.055	1.055	1.039	1.133

The Cambridge Crystallographic Data Centre via www.ccdc.cam.ac.uk/data_request/cif.

Acknowledgments

We thank the National Science Council and the Ministry of Education of the Republic of China for financial support. We are also grateful to Mr. Bor-Wen Shih for his help with magnetic measurement.

[1] a) J. F. Berry, F. A. Cotton, L. M. Daniels, C. A. Murillo, *J. Am. Chem. Soc.* **2002**, *124*, 3212–3213; b) S.-Y. Lin, I.-W. P. Chen, C.-H. Chen, M.-H. Hsieh, C.-Y. Yeh, T.-W. Lin, Y.-H. Chen, S.-M. Peng, *J. Phys. Chem. B* **2004**, *108*, 959–964; c) I.-W. P. Chen, M.-D. Fu, W.-H. Tseng, J.-Y. Yu, S.-H. Wu, C.-J. Ku, C.-H. Chen, S.-M. Peng, *Angew. Chem. Int. Ed.* **2006**, *45*, 5414–5418.

[2] a) E.-C. Yang, M.-C. Cheng, M.-S. Tsai, S.-M. Peng, *J. Chem. Soc., Chem. Commun.* **1994**, 2377–2378; b) C.-K. Kuo, J.-C. Chang, C.-Y. Yeh, G.-H. Lee, C.-C. Wang, S.-M. Peng, *Dalton Trans.* **2005**, 3696–3701; c) R. Clérac, F. A. Cotton, L. M. Daniels, K. R. Dunbar, K. Kirschbaum, C. A. Murillo, A. A. Pinkerton, A. J. Schutz, X. Wang, *J. Am. Chem. Soc.* **2000**, *122*, 6226–6236; d) J. F. Berry, F. A. Cotton, T. Lu, C. A. Murillo, B. K. Roberts, X. Wang, *J. Am. Chem. Soc.* **2004**, *126*, 7082–7096; e) R. H. Ismayilov, W.-Z. Wang, G.-H. Lee, R.-R. Wang, I. P.-H. Liu, C.-Y. Yeh, S.-M. Peng, *Dalton Trans.* **2007**, 2898–2907; f) J. F. Berry, F. A. Cotton, P. Lei, C. A. Murillo, *Inorg. Chem.* **2003**, *42*, 377–382; g) S.-J. Shieh, C.-C. Lin, I. Chao, C.-C. Wang, S.-M. Peng, *Chem. Commun.* **1996**, 315–316; h) F. A. Cotton, L. M. Daniels, C. A. Murillo, I. Pascual, *Inorg. Chem. Commun.* **1998**, *1*, 1–3.

[3] a) S.-Y. Lai, T.-W. Lin, Y.-H. Chen, C.-C. Wang, G.-H. Lee, M.-H. Yang, M.-K. Leung, S.-M. Peng, *J. Am. Chem. Soc.* **1999**, *121*, 250–251; b) F. A. Cotton, L. M. Daniels, C. A. Murillo, X. Wang, *Chem. Commun.* **1998**, 39–40; c) X. López, M.-Y. Huang, G.-C. Huang, S.-M. Peng, F.-Y. Li, M. Bénard, M.-M. Rohmer, *Inorg. Chem.* **2006**, *45*, 9075–9084.

[4] a) S.-J. Shieh, C.-C. Chou, G.-H. Lee, C.-C. Wang, S.-M. Peng, *Angew. Chem. Int. Ed. Engl.* **1997**, *36*, 56–59; b) C.-C. Wang, W.-C. Lo, C.-C. Chou, G.-H. Lee, J.-M. Chen, S.-M. Peng, *Inorg. Chem.* **1998**, *37*, 4059–4065; c) C. Y. Yeh, C. H. Chou, K. C. Pan, C. C. Wang, G. H. Lee, Y. O. Su, S. M. Peng, *J. Chem. Soc., Dalton Trans.* **2002**, 2670–2677; d) J. F. Berry, F. A. Cotton, P. Lei, T. Lu, C. A. Murillo, *Inorg. Chem.* **2003**, *42*, 3534–3539; e) H.-C. Chang, J.-T. Li, C.-C. Wang, T.-W. Lin, H.-C. Lee, G.-H. Lee, S.-M. Peng, *Eur. J. Inorg. Chem.* **1999**, 1243–1251; f) C.-Y. Yeh, Y.-L. Chiang, G.-H. Lee, S.-M. Peng, *Inorg. Chem.* **2002**, *41*, 4096–4098.

[5] a) C.-H. Chien, G.-H. Lee, Y. Song, S.-M. Peng, *Dalton Trans.* **2006**, 3249–3256; b) C.-H. Chien, J.-C. Chang, C.-Y. Yeh, G.-H. Lee, J.-M. Fang, S.-M. Peng, *Dalton Trans.* **2006**, 2106–2113.

[6] a) Y.-H. Chen, C.-C. Lee, C.-C. Wang, G.-H. Lee, S.-Y. Lai, S.-M. Peng, *Chem. Commun.* **1999**, 1667–1668; b) S.-Y. Lai, C.-C. Wang, Y.-H. Chen, C.-C. Lee, Y.-H. Liu, S.-M. Peng, *J. Chin. Chem. Soc.* **1999**, *46*, 477–485; c) W.-Z. Wang, R. H. Ismayilov, G.-H. Lee, I. P.-C. Liu, C.-Y. Yeh, S.-M. Peng, *Dalton Trans.* **2007**, 830–839.

[7] a) S.-M. Peng, C.-C. Wang, Y.-L. Jang, Y.-H. Chen, F.-Y. Li, C.-Y. Mou, M.-K. Leung, *J. Magn. Magn. Mater.* **2000**, *209*, 80–83; b) R. H. Ismayilov, W.-Z. Wang, R.-R. Wang, C.-Y. Yeh, G.-H. Lee, S.-M. Peng, *Chem. Commun.* **2007**, 1121–1123.

[8] C.-Y. Yeh, C.-C. Wang, Y.-H. Chen, S.-M. Peng in *Redox Systems Under Nano-Space Control* (Ed.: T., Hirao), Springer, Germany, **2006**, ch. 5.

[9] M.-Y. Huang, C.-Y. Yeh, G.-H. Lee, S.-M. Peng, *Dalton Trans.* **2006**, 5683–5690.

[10] R. Clérac, F. A. Cotton, L. M. Daniels, K. R. Dunbar, C. A. Murillo, I. Pascual, *Inorg. Chem.* **2000**, *39*, 752–756.

[11] G. M. Sheldrick, *SHELXS-97*, *Program for solution of crystal structures*, University of Göttingen, Germany, **1997**.

[12] G. M. Sheldrick, *SHELXL-97*, *Program for refinement of crystal structures*, University of Göttingen, Germany, **1997**.

Received: January 14, 2009
Published Online: April 2, 2009

